Control of septum thickness by the curvature of SepF polymers

Control of septum thickness by the curvature of SepF polymers

Michaela Wenzel[a,1,2], Ilkay N. Celik Gulsoy[a,2], Yongqiang Gao[a,3], Zihao Teng[a], Joost Willemse[b], Martijn Middelkamp[c], Mariska G. M. van Rosmalen[d], Per W. B. Larsen[e], Nicole N. van der Wel[e], Gijs J. L. Wuite[d], Wouter H. Roos[c], and Leendert W. Hamoen[a,4]

[a]Bacterial Cell Biology, Swammerdam Institute for Life Sciences, University of Amsterdam, 1098 XH Amsterdam, The Netherlands; [b]Molecular Biotechnology, Institute of Biology, Leiden University, 2333 BE, Leiden, The Netherlands; [c]Molecular Biophysics, Zernike Institute, University of Groningen, 9747 AG Groningen, The Netherlands; [d]Department of Physics and Astronomy and Laser Lab, Free University of Amsterdam, 1081 HV Amsterdam, The Netherlands; and [e]Department of Medical Biology, Electron Microscopy Center Amsterdam, Amsterdam UMC, 1105 AZ Amsterdam, The Netherlands

Edited by Joe Lutkenhaus, University of Kansas Medical Center, Kansas City, KS, and approved November 24, 2020 (received for review February 11, 2020)

Gram-positive bacteria divide by forming a thick cross wall. How the thickness of this septal wall is controlled is unknown. In this type of bacteria, the key cell division protein FtsZ is anchored to the cell membrane by two proteins, FtsA and/or SepF. We have isolated SepF homologs from different bacterial species and found that they all polymerize into large protein rings with diameters varying from 19 to 44 nm. Interestingly, these values correlated well with the thickness of their septa. To test whether ring diameter determines septal thickness, we tried to construct different SepF chimeras with the purpose to manipulate the diameter of the SepF protein ring. This was indeed possible and confirmed that the conserved core domain of SepF regulates ring diameter. Importantly, when SepF chimeras with different diameters were expressed in the bacterial host *Bacillus subtilis*, the thickness of its septa changed accordingly. These results strongly support a model in which septal thickness is controlled by curved molecular clamps formed by SepF polymers attached to the leading edge of nascent septa. This also implies that the intrinsic shape of a protein polymer can function as a mold to shape the cell wall.

cell division | *Bacillus subtilis* | SepF | FtsZ

The hallmark of Gram-positive bacteria is their thick cell wall composed of multiple layers of peptidoglycan. They divide by synthesizing a cross wall in between the newly formed daughter cells, and the thickness of the nascent division septum approaches that of the lateral cell wall. How Gram-positive bacteria regulate the thickness of their division septum is not known.

Bacterial cell division is accomplished by a complex multiprotein machinery called the divisome. Assembly of the divisome begins with polymerization of the tubulin homolog FtsZ at midcell into a ring-like configuration, the so-called Z ring (1). This structure forms a scaffold for the late cell division proteins that are responsible for synthesis of the dividing septal wall (2). Several cell division proteins support the formation of the Z ring, and a key step is the anchoring of FtsZ polymers to the cell membrane. This is achieved by the conserved peripheral membrane proteins FtsA and SepF. Both proteins directly interact with FtsZ and use an amphipathic α-helix to bind to the cell membrane (3, 4). FtsA can be found in both Gram-positive and Gram-negative bacteria, whereas SepF is widely conserved in Gram-positive bacteria, cyanobacteria, and also in archaea, but has no known homolog in Gram-negatives (5, 6). Other Z ring proteins are the conserved protein ZapA, which interlinks FtsZ polymers (7), and the bitopic transmembrane proteins EzrA (Gram-positives) and ZipA (Gram-negatives) (8, 9). Once the Z ring is assembled, the late cell division proteins arrive. These conserved transmembrane proteins form a complex comprising the peptidoglycan glycosyltransferase FtsW (10), the transpeptidase Pbp2B (FtsI in Gram-negatives) (11, 12), and the heterotrimeric complex composed of FtsL, DivIC, and DivIB (FtsL, FtsB, and FtsQ in Gram-negatives, respectively) (13, 14). It is assumed that the latter three proteins regulate the assembly of late cell division proteins, although it is not yet clear how the late proteins are recruited to the Z ring in Gram-positive bacteria.

Some bacteria, such as the Gram-positive model organism *Bacillus subtilis*, contain both FtsA and SepF, and this organism needs only one of them for Z ring formation. However, the absence of SepF results in highly deformed septa, which is not the case when FtsA is absent (6). This indicates that SepF must have an additional function related to septum formation. A curious property of purified *B. subtilis* SepF is that it forms large ring structures with an inner diameter of 40 nm (15). Based on the SepF crystal structure, these rings must encompass at least 80–100 SepF molecules (15). In vitro, these protein rings are able to bundle FtsZ polymers into very long microtubule-like structures with SepF rings stacked perpendicularly to the FtsZ polymers (16). However, such microtubular structures have never been observed in bacteria, and later studies showed that the membrane-binding amphipathic α-helix of SepF is likely located inside the ring, which seems to rule out ring formation in vivo (15).

Interestingly, the inner diameter of SepF rings is about the same size as the thickness of the septal wall (43 nm). We

Significance

Many bacteria form a thick cell wall and divide by forming a cross wall. How they control the thickness of their cell wall and cross wall is unknown. In this study, we show that in these bacteria the cell division protein SepF forms very large protein rings with diameters that correspond to the diameter of their cross walls. Importantly, when we changed the diameter of SepF rings in the bacterial host *Bacillus subtilis*, the thickness of its cross wall changed accordingly. These results provide strong evidence that a large protein ring can function as a mold to control the thickness of the cell wall that divides these bacterial cells.

Author contributions: M.W. and L.W.H. designed research; M.W., I.N.C.G., Y.G., Z.T., J.W., M.M., M.G.M.v.R., P.W.B.L., N.N.v.d.W., G.J.L.W., and W.H.R. performed research; M.W., I.N.C.G., Y.G., Z.T., J.W., M.M., M.G.M.v.R., P.W.B.L., N.N.v.d.W., G.J.L.W., W.H.R., and L.W.H. analyzed data; and M.W. and L.W.H. wrote the paper.

The authors declare no competing interest.

This article is a PNAS Direct Submission.

[1]Present address: Division of Chemical Biology, Department of Biology and Biological Engineering, Chalmers University of Technology, 412 96 Gothenburg, Sweden.

[2]M.W. and I.N.C.G. contributed equally to this work.

[3]Present address: Department of Microbiology and Immunobiology, Harvard Medical School, Boston, MA 02115.

[4]To whom correspondence may be addressed. Email: l.w.hamoen@uva.nl.

This article contains supporting information online at https://www.pnas.org/lookup/suppl/doi:10.1073/pnas.2002635118/-/DCSupplemental.

Published December 21, 2020.

wondered whether this relationship is relevant and, if so, whether SepF rings might actually control the thickness of the septum. To examine this, we purified SepF from different Gram-positive bacteria and found that all these proteins bind to lipid membranes and form large protein rings, albeit with different diameters. Importantly, also in these organisms there was a correlation between SepF ring diameter and septum thickness. To confirm that the SepF ring diameter determines septal width, we expressed SepF chimeras with larger and smaller diameters in *B. subtilis*. Indeed, this changed the thickness of septa accordingly. These results provide strong evidence that Gram-positive bacteria regulate the thickness of their septal wall by the strong curvature of SepF polymers at the leading edge of nascent septa. This also implies that the intrinsic form of a protein polymer can function as a mold that can shape a cell wall.

Results

SepF Rings and Tubules. Purified *B. subtilis* SepF forms large protein rings when observed with transmission electron microscopy (TEM) using negative staining with uranyl acetate (15). To confirm these findings with an independent method, we examined whether the protein can form rings under more physiological conditions using atomic force microscopy (AFM). It appeared that under these conditions purified *B. subtilis* SepF also forms rings with average diameters of 41 nm (Fig. 1 *A* and *B* and *SI Appendix*, Fig. S1). Rings were 2–4 nm high (Fig. 1 *C* and *D*), which corresponds to a single or double molecule stacking, since the crystal packing has shown that SepF polymers can be either 1.5 or 2.6 nm wide, depending on the orientation of SepF dimers (15).

Previously, SepF was purified as a maltose-binding protein (MBP) fusion followed by proteolytic cleavage and removal of MBP using ion-exchange chromatography (15, 16). We noticed that after cleavage, SepF precipitates, possibly due to the presence of calcium in the digestion buffer. After resuspension in calcium-free buffer, SepF formed stacks and tubules with diameters corresponding to that of SepF rings when observed by TEM (Fig. 1*E*). After ion-exchange chromatography, only rings were found (Fig. 1*F*). These findings, together with the AFM data, show that the circular polymerization of *B. subtilis* SepF is a robust characteristic, at least in vitro.

SepF from Other Species. To determine whether ring formation is a conserved feature of SepF, we purified the protein from different organisms. *Bacillus cereus* is an important food-spoiling bacterium (17, 18) and the causative agent of rainforest anthrax (19–21). *Bacillus megaterium* is a particularly large *Bacillus* species. These two bacteria were chosen as close relatives of *B. subtilis*. We further selected *Clostridium perfringens*, *Mycobacterium tuberculosis*, and *Streptococcus pneumoniae,* all of which are important human pathogens. *S. pneumoniae* differs from the rest since it forms cocci instead of rods, and *M. tuberculosis* is one of the bacterial species that lack an FtsA homolog. An amino acid sequence alignment of the different SepF homologs is shown in *SI Appendix*, Fig. S2. The central core domain of the protein, which contains the FtsZ binding site and is essential for polymerization of SepF into a ring (15), is particularly conserved (*SI Appendix*, Fig. S2 and Tables S1 and S2). All proteins were successfully purified as MBP fusions. *B. megaterium, C. perfringens, M. tuberculosis,* and *S. pneumoniae* SepF precipitated after proteolytic cleavage from MBP and were collected by centrifugation, whereas *B. cereus* SepF was more soluble and was therefore isolated by ion-exchange chromatography.

Membrane Binding. A key property of *B. subtilis* SepF is its capacity to bind to the cell membrane, which is achieved by an N-terminal amphipathic α-helix (amino acids 1–13) (15). This N-terminal amphipathic helix is reasonably conserved in the different SepF variants (*SI Appendix*, Fig. S2 and see *SI Appendix*, Fig. S3 for helical wheel depictions), although the helices differ in their hydrophobicity and hydrophobic moment (*SI Appendix*, Fig. S4). To confirm that the different SepF molecules are able to bind to lipid membranes, the purified proteins were mixed with liposomes. This caused a strong aggregation of liposomes, and deformed them into small vesicles, when observed with high-resolution structured illumination microscopy (SIM). One example, *S. pneumoniae* SepF, is presented in Fig. 2 *A* and *B* (see *SI Appendix*, Fig. S5 for all variants). Such liposome deformation is a typical characteristic of membrane-interacting amphipathic α-helices (22), and a *B. subtilis* SepF variant without the N-terminal α-helix does not possess this property (15). These results indicate that the membrane binding activity of SepF is conserved.

Ring Formation. Another characteristic of *B. subtilis* SepF is its tendency to polymerize into a curved structure. If this feature is important for the activity of SepF, it should not be restricted to the *B. subtilis* protein. To check this, the purified SepF homologs were spotted on TEM grids and negatively stained with uranyl acetate. Indeed, as shown in Fig. 2*C*, all SepF variants formed large protein rings. Rings from any given species were of a remarkably constant size (Fig. 2*E*). However, the ring diameters differed considerably between the species, ranging from 19 up to 44 nm (Fig. 2 *E* and *H*).

Correlation with Septum Thickness. The different ring diameters provided a first support for our hypothesis that SepF ring diameter might regulate septum thickness. To confirm this, we performed TEM of the different bacterial species and measured the thickness of their nascent cell division septa (Fig. 2 *D* and *F*). As shown in Fig. 2*G*, there is a clear correlation between inner ring diameter and the thickness of septa in the different species. Due to the granular ultrastructure of *B. megaterium* cells, which makes TEM staining difficult, we did not succeed in measuring nascent septa in this organism. However, we could measure some closed septa, which were significantly thicker compared to those of *B. subtilis* (*SI Appendix*, Fig. S7). Similarly, we did not observe septa in *M. tuberculosis* samples, probably due to their extremely slow growth and "snapping" separation mechanism (23). Therefore, we used published data of nascent *M. tuberculosis* septa for our comparison (24). In both cases, we observed the same trend as for the other samples, small rings coincide with thin septa (*M. tuberculosis*) and large rings with thick septa (*B. megaterium*). Only *B. cereus* did not follow this trend, with SepF rings that are significantly smaller than the width of its septa (Fig. 2 *G* and *H*).

Core Domain Defines Ring Diameter. Proteolytic trimming has shown that the core domain of *B. subtilis* SepF, spanning amino acids 57–151, is sufficient for the formation of rings (15). Therefore, we assumed that this core domain determines ring diameter. To test this, we replaced the conserved core domain of *B. subtilis* SepF with those of the SepF proteins from the other species, maintaining the first 67 and last 13 amino acids of *B. subtilis* SepF (*SI Appendix*, Fig. S2). These chimeras were then expressed in *Escherichia coli*, purified, and visualized by TEM using negative staining. All SepF chimeras were able to form rings. Importantly, the ring diameters of these chimeras corresponded very well to the diameters of the original SepF variants, without exception (Fig. 3).

Functional Chimeras. If it is true that the diameter of SepF rings determines the thickness of septa, then expressing a SepF variant with a smaller or larger ring diameter in *B. subtilis* should result in thinner or thicker septa. It is unlikely that SepF from other species function in *B. subtilis*, since the N and C termini of SepF, which are much less conserved, are crucial for its activity (15, 16). Therefore, our chimeras provided a unique opportunity to test

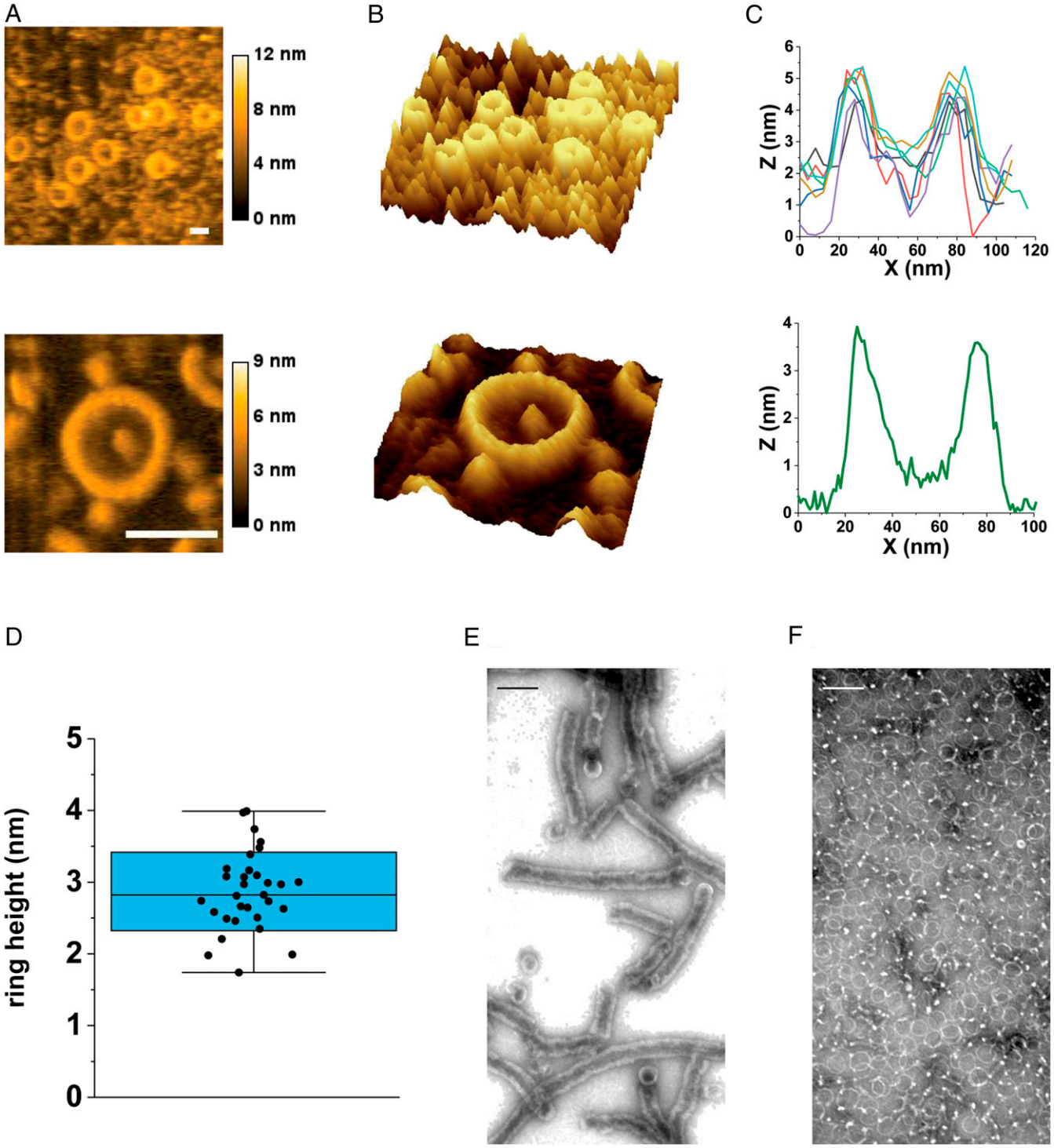

Fig. 1. SepF forms rings and tubules. (*A*) Plane AFM images of different SepF rings imaged in buffer solution. (*B*) Three-dimensional projections of the same images. (*C*) Height profiles of individual SepF rings shown in *A* and *B*. (*D*) Height measurements of SepF rings derived from AFM data ($n = 31$). The blue box reflects the SD, and the whisker indicates the range of the outliers. (*E*) TEM image of SepF stack and tubules after cleavage from MBP. (*F*) TEM image of SepF rings after ion-exchange chromatography. (Scale bars: *A*, 50 nm; *E* and *F*, 100 nm.)

this. All chimera proteins were expressed in *B. subtilis* from the isopropyl-β-D-thiogalactoside (IPTG)-inducible *Pspac* promoter in similar levels as the WT protein (*SI Appendix*, Fig. S8). To determine whether they are active in *B. subtilis*, the chimera proteins were expressed in a Δ*sepF* strain. *B. subtilis* is one of the few species that can grow without SepF, although this leads to strongly deformed septa (6). Since these deformed septa are lined by the cytoplasmic membrane, this phenotype can be easily observed using high-resolution SIM microscopy by fluorescently labeling the cell membrane (Fig. 4*A*). Only the *S. pneumoniae* chimera failed to rescue the Δ*sepF* phenotype, while the *B. cereus, B. megaterium, C. perfringens,* and *M. tuberculosis* chimeras were all able to restore normal septum formation in the Δ*sepF* background (Fig. 4*A*). To check that the membrane

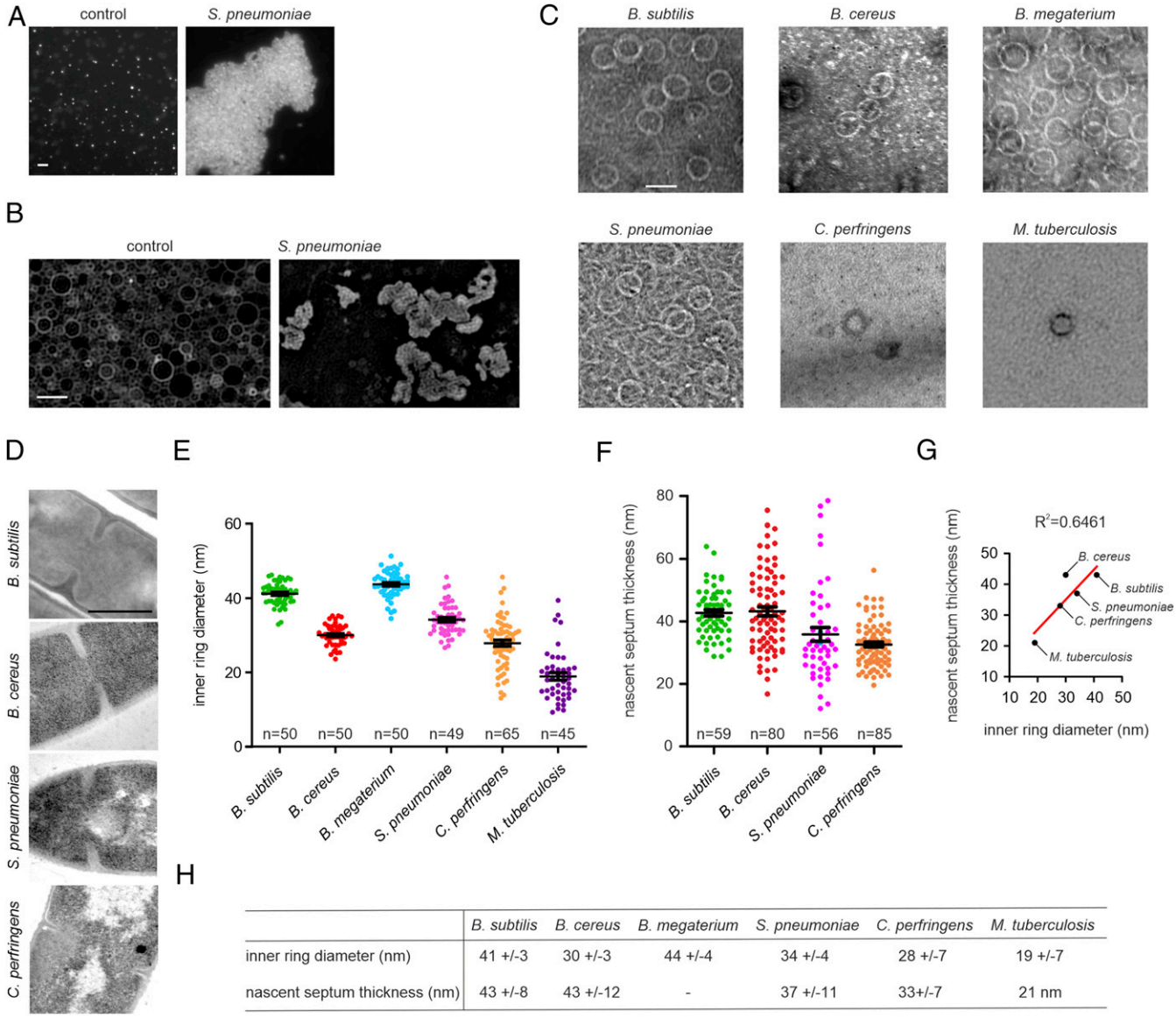

H

	B. subtilis	*B. cereus*	*B. megaterium*	*S. pneumoniae*	*C. perfringens*	*M. tuberculosis*
inner ring diameter (nm)	41 +/-3	30 +/-3	44 +/-4	34 +/-4	28 +/-7	19 +/-7
nascent septum thickness (nm)	43 +/-8	43 +/-12	-	37 +/-11	33+/-7	21 nm

Fig. 2. Membrane binding, ring formation, and septum thickness. (*A*) Fluorescence light microscopy image showing the aggregation of small liposomes (~200 nm) by purified *S. pneumoniae* SepF. Liposomes were stained with Nile red. (*B*) SIM image showing deformation of large liposomes (800 nm) by purified *S. pneumoniae* SepF. Liposomes were stained with mitotracker green. SepF (0.25 mg/mL) was mixed with 2 mg/mL liposomes. See *SI Appendix*, Fig. S5 for the results with other SepF variants. (*C*) TEM pictures of purified SepF from the different species. See *SI Appendix*, Fig. S6 for more rings from *C. perfringens* and *M. tuberculosis* samples. (*D*) TEM images of nascent cell division septa of the respective species. (*E*) Quantification of the inner SepF ring diameter. Ring diameter was consistently measured as the inner diameter of the SepF ring at its widest point. Black bars show mean with SEM. Number of measured rings is indicated in the graph. (*F*) Quantification of the thickness of the nascent septa of the respective organisms. Black bars show mean with SEM. Number of measured septa is indicated in the graphs. (*G*) Correlation between inner SepF ring diameter and septum thickness. Coefficient of determination is indicated above the graph. (*H*) Comparison of inner ring diameters with nascent septum thickness. Average ± SDs is indicated. Septum thickness data for *M. tuberculosis* were taken from the literature (24). For *B. megaterium*, no nascent septa were observed. For measurements of closed septa, see *SI Appendix*, Fig. S7. (Scale bars: *B*, 1 μm; *C*, 50 nm; *D*, 500 nm.)

deformations observed by SIM are indeed indicative of deformed cell wall septa, we confirmed these findings by TEM (Fig. 4*B*).

SepF Core Domain Regulates Septum Thickness. We then proceeded to measure nascent septa of the *B. subtilis* strains expressing the respective chimera proteins. The inner ring diameter of the *C. perfringens* SepF chimera (24 nm) is considerably smaller than *B. subtilis* SepF (42 nm). When this chimera was expressed in the Δ*sepF* strain, the septum thickness decreased substantially from 43 to 28 nm (Fig. 4 *C* and *D*). A similar decrease in septum thickness was observed, when the *M. tuberculosis* SepF chimera (35 nm diameter) was expressed in the Δ*sepF* background (Fig. 4 *C–E*). However, when expressing the larger *B. megaterium* chimera (48 nm), the nascent septum width increased to 50 nm (Fig. 4 *C–E*). These results strongly suggest that the SepF ring diameter controls nascent septum thickness.

The only variant that behaved differently was the *B. cereus* chimera. The diameter of *B. cereus* SepF and the *B. cereus* SepF chimera rings is ~10 nm smaller than *B. subtilis* SepF rings (Figs. 2*F* and 3 *B* and *C*), yet expression of the *B. cereus* chimera in *B. subtilis* Δ*sepF* resulted in septa with a thickness comparable to

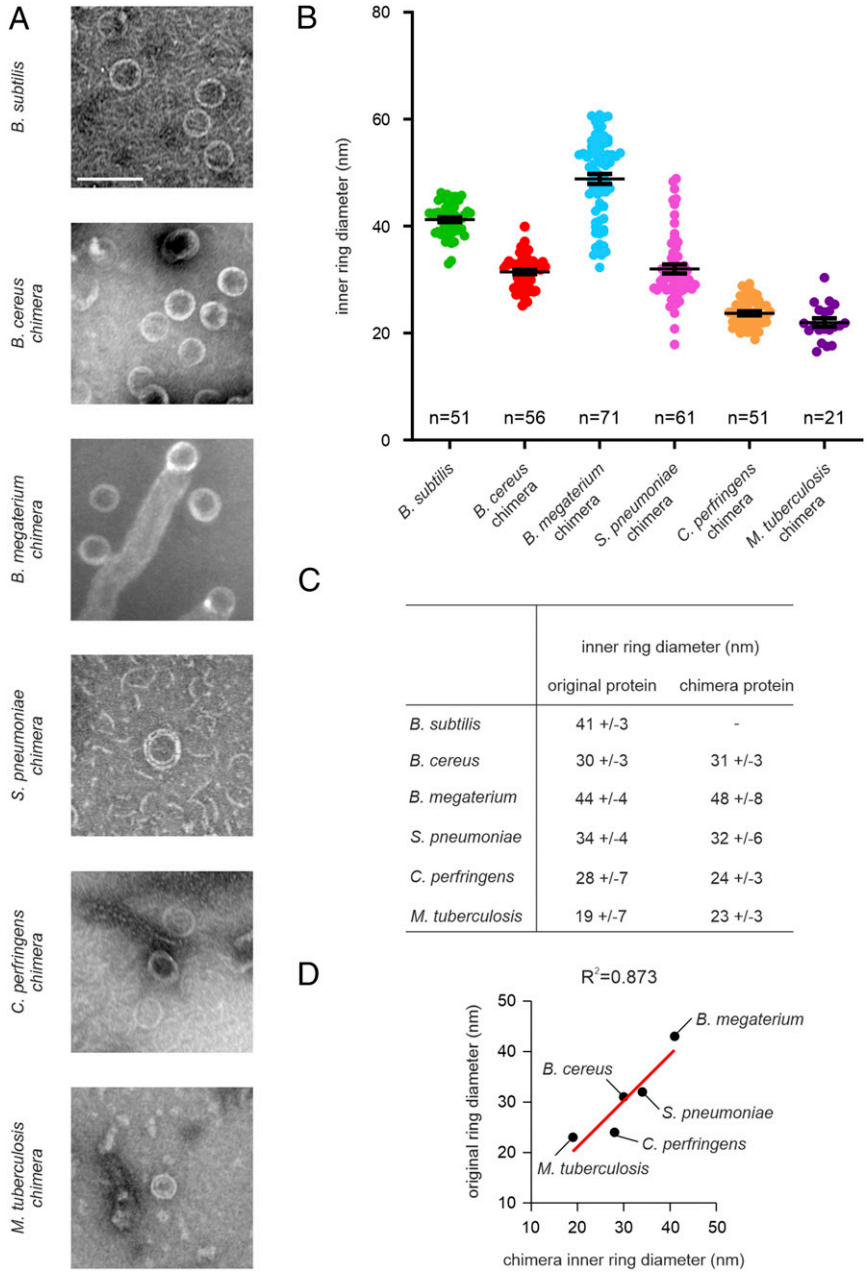

	inner ring diameter (nm)	
	original protein	chimera protein
B. subtilis	41 +/-3	-
B. cereus	30 +/-3	31 +/-3
B. megaterium	44 +/-4	48 +/-8
S. pneumoniae	34 +/-4	32 +/-6
C. perfringens	28 +/-7	24 +/-3
M. tuberculosis	19 +/-7	23 +/-3

Fig. 3. The conserved core domain of SepF determines ring diameter. (*A*) TEM pictures of purified SepF chimera proteins. (Scale bar, 100 nm.) (*B*) Quantification of ring diameter. Black bars represent mean with SEM. A minimum of 50 rings was measured. (*C*) Comparison of the inner ring diameters of the original and chimera proteins. Average ± SD is given. Number of measured rings is indicated in the graphs. (*D*) Correlation between original and chimera ring diameter. Coefficient of determination is indicated above the graph.

that of WT *B. subtilis* cells (Fig. 4 *C–E*). However, since *B. cereus* cells themselves have a septum thickness comparable to that of *B. subtilis* (both ~43 nm, Fig. 2*G*), this result is still consistent with the assumption that the core domain of SepF determines septum thickness.

Discussion

In this study, we have shown that the membrane binding and ring forming activities are conserved in SepF homologs, the correlation between ring diameter and septum thickness can be found in different Gram-positive bacteria, and the septum thickness of *B. subtilis* cells can be reduced or increased by expressing SepF mutants with a smaller or larger diameter. Together these findings strongly suggest that the diameter of curved SepF polymers is an important determinant of septum thickness.

The positioning of SepF polymers at the division site cannot be directly observed using high-resolution cryo-electron microscopy due to the electron density of the bacterial cytoplasm and cell wall. However, our findings provide support for a SepF clamp model (Fig. 5). Since the membrane-binding amphipathic α-helix of SepF is located inside the ring, it is likely that SepF polymers do not form rings, but instead form arcs, wrapping the leading edge of nascent septa, on top of which FtsZ polymers bind and align (15). Since these arcs control the freedom of movement of FtsZ polymers, including the peptidoglycan synthetic apparatus that is linked to them, the diameter of SepF rings will regulate the thickness of the septal wall. In this model,

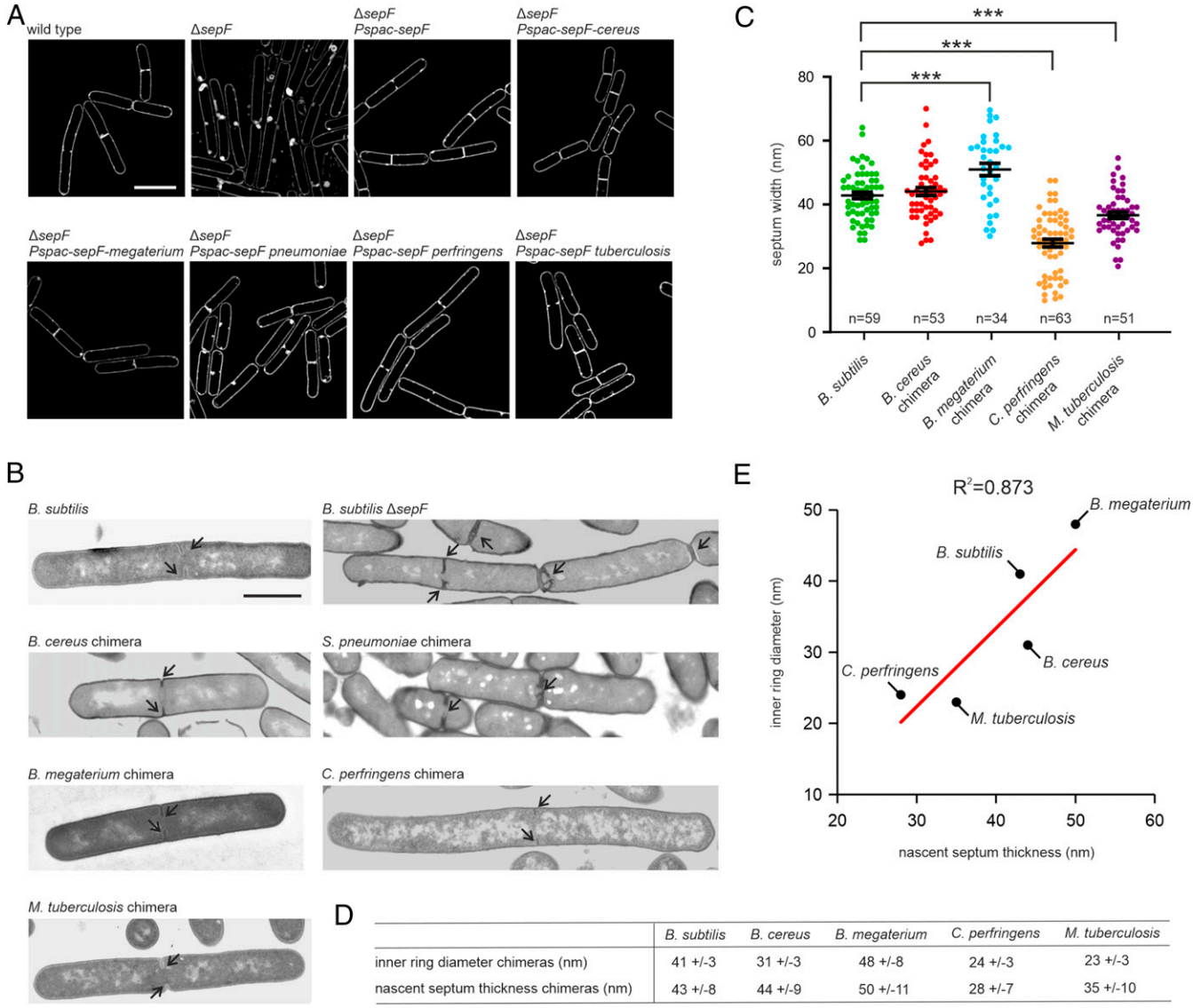

D

	B. subtilis	*B. cereus*	*B. megaterium*	*C. perfringens*	*M. tuberculosis*
inner ring diameter chimeras (nm)	41 +/-3	31 +/-3	48 +/-8	24 +/-3	23 +/-3
nascent septum thickness chimeras (nm)	43 +/-8	44 +/-9	50 +/-11	28 +/-7	35 +/-10

Fig. 4. SepF ring diameter regulates septum thickness. (*A*) SIM images of *B. subtilis* Δ*sepF* cells expressing different SepF chimeras. The chimeras were expressed from the IPTG-inducible *Pspac* promotor. As a control we included the complementation strain expressing WT *sepF* from the same promoter. Cells were grown in the presence of 100 μM IPTG until midlog phase prior to membrane staining and microscopy. Lack of SepF results in severely deformed septa, which shows as highly fluorescent membrane patches due to membrane invaginations and double membranes. (*B*) Representative TEM images of septa of Δ*sepF* strains expressing the different SepF chimeras. (*C*) Quantification of the septum thickness of the different strains. Black bars represent mean with SEM. *P* values for *B. megaterium*, *C. perfringens,* and *M. tuberculosis* chimeras compared to *B. subtilis* are <0.0001. Number of measured septa is indicated in the graphs. Comparison (*D*) and correlation (*E*) of the inner ring diameter of SepF chimeras and nascent septum thickness of *B. subtilis* Δ*sepF* expressing the chimeras, or an IPTG-inducible WT *sepF* as control. Coefficient of determination is indicated above the graph. (Scale bars: *A*, 2 μm; *B*, 1 μm.)

many SepF arcs must line the leading edge of the nascent septum to maintain an even thickness. This could be facilitated by the propensity of SepF rings to form stacks (Fig. 1*F*).

B. cereus SepF behaved slightly different and showed an average inner ring diameter of 30 nm, which is smaller than its average septum thickness of 43 nm. The corresponding chimera protein with 30-nm diameter produced 44-nm-thick septa in *B. subtilis*. This suggests that also in *B. cereus* the SepF core domain regulates septum thickness, although not exclusively by the physical confinement of SepF polymers. Possibly, *B. cereus* SepF polymers are more flexible in a cellular environment, enabling a wider diameter. Alternatively, other proteins could be involved in controlling septum diameter. In fact, *B. subtilis* can still make septa, albeit irregular in shape, when SepF is absent, suggesting that other factors provide some control of FtsZ polymers. FtsA, which also forms polymers and is capable of deforming membranes (25, 26), might be such a factor. *E. coli* FtsA has been shown to form ring structures in vitro as well (25). However, the inner diameter of these rings is only ∼15 nm. Whether *B. subtilis* FtsA can polymerize into much larger rings is unknown. However, the fact that neither a deletion of *ftsA* nor any other known cell division gene results in similar septal deformations as a *sepF* deletion in *B. subtilis*, together with our finding that septum width can be manipulated by changing SepF ring diameter, suggests that SepF is a key player in regulating septum thickness.

Gram-negative bacteria contain a cell wall that consists of a single layer of peptidoglycan. The lipoproteins LpoA and LpoB, which reach through the peptidoglycan layer to contact and regulate the cell membrane-anchored peptidoglycan-synthetic enzymes, are thought to regulate peptidoglycan thickness in

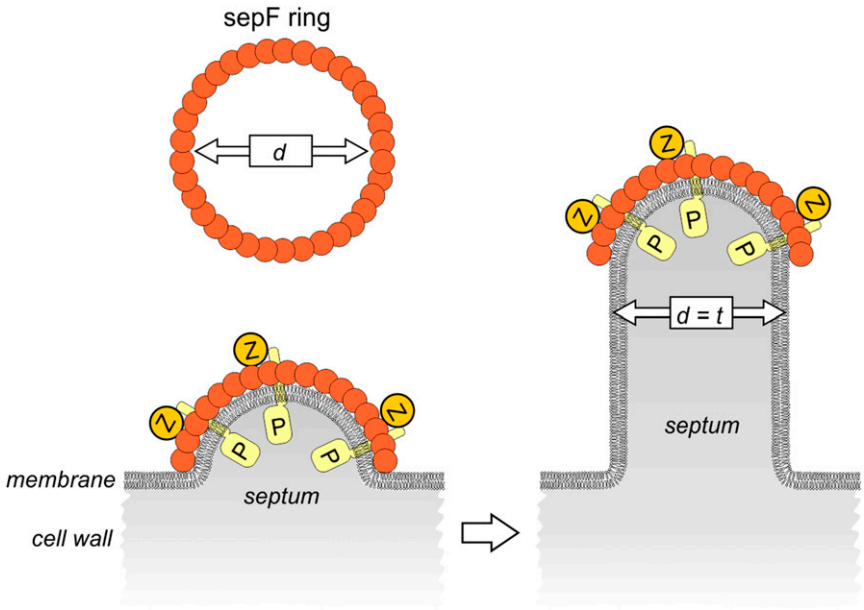

Fig. 5. Clamp model illustrating how SepF polymers can control septal thickness. SepF forms large rings with an average inner ring diameter (*d*) that corresponds to the thickness of septa (*t*). Cross-sections of a nascent septum (gray) is depicted. FtsZ polymers (Z) bind to the outside of SepF rings, in a perpendicular fasion. The transmembrane peptidoglycan synthesis machinery (P) is associated with FtsZ polymers. Of note, it is not yet known how these transmembrane proteins are linked to FtsZ polymers in Gram-positive bacteria, and this association might be indirect.

these species (27). Possibly, this is why Gram-negative bacteria do not need a SepF-like protein for septum thickness control.

Regulation of the shape of septal walls by SepF through its intrinsic curvature is to some degree reminiscent of the activity of MreB, which controls the rod shape of many bacteria (28). MreB forms polymers of defined curvature that orientate and move transversely to the long axis of cells, along the direction of greatest membrane curvature (29), thereby guiding the cell wall synthetic machinery in a way that enforces and maintains a rod shape (30, 31). However, unlike SepF, the intrinsic curvature of MreB filaments, which has been estimated to have a diameter of roughly 200 nm (29), does not correlate with the diameter of the cell, which is much larger (29). It is assumed that the much stronger curvature of MreB filaments in comparison to the curvature of the cell deforms the cell membrane as MreB filaments bind to it, thereby enforcing the alignment of the filaments perpendicular to the long axis of the cell (29, 32). This is a very different molecular mechanism than the molecular clamp model of SepF, which is based on spatial confinement of peptidoglycan synthesis by the protein arc. Moreover, MreB binds to the membrane with the convex side of the polymer, while the membrane-binding domain of SepF is located on the concave side (15). In conclusion, the control of septum thickness by a molecular clamp, such as a SepF arc, is a distinct concept of how protein polymers can control the shape of growing cell walls.

Materials and Methods

Strain Construction. All strains used in this study are listed in *SI Appendix*, Table S3, plasmids in *SI Appendix*, Table S4, and primers in *SI Appendix*, Table S5. Accession numbers of the different *sepF* sequences are listed in *SI Appendix*, Table S6. Plasmids for purification of SepF variants were constructed by PCR amplification of *sepF* from the respective organism DNA, followed by restriction cloning into the pMalC2 plasmid (33), using the XbaI and SmaI or EcoRI restriction sites. pMalC2-based plasmids for purification of chimera proteins and pAPNC-213-kan–based plasmids (34) for integration of *sepF* variants into the *aprE* locus in the *B. subtilis* genome were constructed by Gibson assembly (35). pMalC2-derived purification plasmids were transformed into calcium-competent *E. coli* BL21 (DE3). pAPNC-213-kan–derived integration plasmids were transformed into *B. subtilis* 168 using a standard starvation protocol (36). Deletions of the *sepF* gene were introduced by transforming the resulting *B. subtilis* strains with chromosomal DNA isolated from YK204 (*sepF::spc*) (37) or BFA2863 (*sepF::ery*) (6), respectively.

Protein Purification. *E. coli* BL21 (DE3) strains carrying pMalC2 plasmids for purification of SepF variants were grown overnight in Luria–Bertani (LB) broth containing 100 μg/mL ampicillin at 37 °C under continuous shaking. Cultures were diluted 1:100 and allowed to grow until an OD_{600} of 0.4 in the presence of ampicillin. Expression of MBP-tagged SepF proteins was induced by addition of 0.5 mM IPTG. Cells were harvested by centrifugation after 4 h of induction and subsequently washed in phosphate-buffered saline supplemented with 1 mM phenylmethylsulfonyl fluoride (PMSF) to prevent protein degradation. Cell pellets were flash-frozen in liquid nitrogen and stored at −80 °C until further use. Cell pellets were resuspended in buffer AF (50 mM Tris·HCl, pH 7.4, 200 mM KCl, 5 mM ethylenediaminetetraacetic acid (EDTA), 0.5 mM dithiothreitol (DTT)) supplemented with one Complete mini protease inhibitor tablet (Roche) and disrupted by French Press. Cell debris was removed by ultracentrifugation at 31,000 × *g*, and the resulting supernatant was filtered through 0.2-μm filter membranes prior to loading onto a Tricorn 10/20 column (GE Healthcare) packed with 2 mL of amylose resin (New England Biolabs) equilibrated with buffer AF. After loading, the column was washed with 5 column volumes buffer AF, followed by buffer BF (50 mM Tris·HCl, pH 7.4) until the baseline was stable. MBP-tagged SepF variants were eluted with buffer BF containing 10 mM maltose. Appropriate fractions were pooled and digested with factor Xa protease (New England Biolabs) in the presence of 2 mM $CaCl_2$ at 4 °C overnight. *B. cereus* SepF was soluble while the others precipitated after cleavage (*B. subtilis, B. megaterium, S. pneumoniae, C. perfringens, M. tuberculosis,* all chimera proteins) due to the presence of calcium. Insoluble proteins were separated from soluble MBP and factor Xa by centrifugation at 10,000 × *g*. Pellets containing pure SepF were dissolved in buffer BF without $CaCl_2$, flash-frozen in liquid nitrogen, and stored at −80 °C until further use. SepF variants that were soluble after factor Xa cleavage were separated from MBP and Factor Xa protease by ion exchange chromatography. To this end, digested samples were loaded onto a 1-mL HiTrap Q column (GE Healthcare) equilibrated with buffer BF. The column was washed with buffer BF until the baseline was stable, followed by washing with 7.5% buffer CF (50 mM Tris·HCl, pH 7.4, 1 M KCl), resulting in elution of MBP, and washing with 17.5% buffer CF, resulting in elution of factor Xa. Pure SepF was eluted with 50% buffer CF, flash-frozen in liquid nitrogen, and stored at −80 °C.

Atomic Force Microscopy. Purified *B. subtilis* SepF was diluted 1:10 in adsorption buffer (110 mM NaCl, 25 mM $MgCl_2$, 10 mM N-(2-hydroxyethyl)piperazine-N′-(2-ethanesulfonic acid) (HEPES), pH 7.5) to enhance the adsorption of the rings onto a freshly cleaved mica surface (Fig. 1). After 30-min incubation at room temperature, an excess of buffer BF was added, and imaging started. Images were taken with a high-speed atomic force microscope (HS-AFM) from RIBM (Japan) operated in amplitude modulation tapping mode in liquid (38, 39). Short cantilevers (USC-F1.2-k0.15, NanoWorld) with spring constant of 0.15 N/m were used. Control experiments on Highly Ordered Pyrolytic Graphite (HOPG) are shown in *SI Appendix*, Fig. S1.

Fluorescence Light Microscopy of Liposomes. Liposomes were prepared from *E. coli* polar lipid extract (Avanti Polar Lipids) as described previously (3). Liposomes were extruded through 0.2-μm filters. Samples were stained with 1 μg/mL Nile red, spotted on 1.2% agarose films, covered with polydopamine–coated coverslips (40), and immediately imaged with a Nikon Eclipse Ti equipped with a CFI Plan Apochromat DM 100× oil objective, an Intensilight HG 130 W lamp, a C11440-22CU Hamamatsu ORCA camera, and NIS elements software. Images were analyzed using ImageJ (NIH).

SIM Microscopy. Liposomes for SIM were prepared from *E. coli* polar lipid extract (Avanti Polar Lipids) as described previously (3). Liposomes were extruded through 0.8-μm filters to obtain large enough vesicles. Subsequently, 0.25 mg/mL of the respective SepF variants was mixed with 2 mg/mL liposomes in SepF binding buffer. Samples were stained with 0.5 μg/mL mitotracker green, spotted on 1.2% agarose films, covered with polydopamine–coated coverslips (40), and immediately imaged with a Nikon Eclipse Ti N-SIM E microscope setup equipped with a CFI SR Apochromat TIRF 100× oil objective (N.A. 1.49), a LU-N3-SIM laser unit, an Orca-Flash 4.0 sCMOS camera (Hamamatsu Photonics K.K.), and NIS elements Ar software. SIM microscopy of bacteria was performed by staining cells with 0.5 μg/mL mitotracker green for 1 min, spotted on a thin film of 1.2% agarose (21).

TEM of Proteins. Protein samples were spotted on glow-discharged 200 mesh formvar/carbon-coated copper grids (Agar Scientific) and incubated for 1 min at room temperature. Excess liquid was removed with paper tissue and samples were negatively stained by adding 100 μL of 2% uranyl acetate drop by drop. Excess staining solution was removed with paper tissue and samples were allowed to air dry. Samples were examined with a JEOL1010 at 60 kV and a Thermo Fisher Tecnai T12 at 120 kV.

Growth Conditions for Microscopy. *B. cereus, S. pneumoniae*, and *C. perfringens* were grown on tryptic soy agar plates containing 5% sheep blood (BioMerieux). After 3 days of aerobic (*B. cereus* and *S. pneumoniae*) or anaerobic incubation (*C. perfringens*) at 37 °C, colonies were transferred to fresh plates and incubated for another 48 h prior to suspension in phosphate-buffered saline and preparation for electron microscopy. *B. megaterium* and all *B. subtilis* strains were grown in LB broth at 37 °C under steady agitation. The medium was supplemented with 0.1 mM IPTG to induce expression of SepF variants, where appropriate. It is important not to use more IPTG since SepF overproduction causes membrane deformations that obscure septa (41). Overnight cultures were grown with appropriate antibiotic concentrations (100 μg/mL spectinomycin, 10 μg/mL chloramphenicol, 5 μg/mL kanamycin, 1 μg/mL erythromycin), where necessary. Overnight cultures were used to inoculate fresh LB containing IPTG but no antibiotics. These cultures were then grown until exponential phase (OD_{600} = 0.4) prior to microscopy.

TEM of Bacteria. Electron microscopy of bacteria was performed according to van Wezel et al (42). (*B. cereus*, *S. pneumoniae*, *C. perfringens)* or to a novel method that uses immobilization of bacterial cells in one plane on an agarose layer prior to fixation and embedding (43, 44) (*B. subtilis, B. megaterium*). Samples were examined with a JEOL 1010 at an electron voltage of 60 kV.

Data Availability. All study data are included in the article and supporting information.

ACKNOWLEDGMENTS. We thank Zehui Zhang and Daniel Antwi-berko for help with sample preparation, Wiep Klaas Smits for help with growing strains, Marien P. Dekker and Jan R. T. van Weering for support with TEM, Sourav Maity for help with HS-AFM, and Gaurav Dugar for critically reading the manuscript. Electron microscopy was performed at the electron microsopy facility of the Free University Amsterdam and Free University Medical Center, supported by the Netherlands Organization for Scientific Research (NWO, middelgroot 91111009), and the Electron Microscopy Center Amsterdam. This work was financially supported by NWO STW-Vici 12128 (to L.W.H.) and NWO-Vidi and NWO Excellent Chemisch Onderzoek (ECHO) (W.H.R.). Y.G. and Z.T. were supported by PhD fellowships from the China Scholarship Council, and M.W. was supported by a postdoc stipend from the Amsterdam Infection and Immunity Institute.

1. J. Lutkenhaus, S. Pichoff, S. Du, Bacterial cytokinesis: From Z ring to divisome. *Cytoskeleton (Hoboken)* **69**, 778–790 (2012).
2. P. Gamba, J. W. Veening, N. J. Saunders, L. W. Hamoen, R. A. Daniel, Two-step assembly dynamics of the Bacillus subtilis divisome. *J. Bacteriol.* **191**, 4186–4194 (2009).
3. H. Strahl, L. W. Hamoen, Membrane potential is important for bacterial cell division. *Proc. Natl. Acad. Sci. U.S.A.* **107**, 12281–12286 (2010).
4. S. Pichoff, J. Lutkenhaus, Tethering the Z ring to the membrane through a conserved membrane targeting sequence in FtsA. *Mol. Microbiol.* **55**, 1722–1734 (2005).
5. J. Errington, R. A. Daniel, D.-J. Scheffers, Cytokinesis in bacteria. *Microbiol. Mol. Biol. Rev.* **67**, 52–65 (2003).
6. L. W. Hamoen, J. C. Meile, W. de Jong, P. Noirot, J. Errington, SepF, a novel FtsZ-interacting protein required for a late step in cell division. *Mol. Microbiol.* **59**, 989–999 (2006).
7. F. J. Gueiros-Filho, R. Losick, A widely conserved bacterial cell division protein that promotes assembly of the tubulin-like protein FtsZ. *Genes Dev.* **16**, 2544–2556 (2002).
8. P. A. Levin, I. G. Kurtser, A. D. Grossman, Identification and characterization of a negative regulator of FtsZ ring formation in Bacillus subtilis. *Proc. Natl. Acad. Sci. U.S.A.* **96**, 9642–9647 (1999).
9. C. A. Hale, P. A. de Boer, Direct binding of FtsZ to ZipA, an essential component of the septal ring structure that mediates cell division in E. coli. *Cell* **88**, 175–185 (1997).
10. A. Taguchi *et al*., FtsW is a peptidoglycan polymerase that is functional only in complex with its cognate penicillin-binding protein. *Nat. Microbiol.* **4**, 587–594 (2019).
11. R. A. Daniel, E. J. Harry, J. Errington, Role of penicillin-binding protein PBP 2B in assembly and functioning of the division machinery of Bacillus subtilis. *Mol. Microbiol.* **35**, 299–311 (2000).
12. L. Wang, M. K. Khattar, W. D. Donachie, J. Lutkenhaus, FtsI and FtsW are localized to the septum in Escherichia coli. *J. Bacteriol.* **180**, 2810–2816 (1998).
13. R. A. Daniel, M.-F. Noirot-Gros, P. Noirot, J. Errington, Multiple interactions between the transmembrane division proteins of Bacillus subtilis and the role of FtsL instability in divisome assembly. *J. Bacteriol.* **188**, 7396–7404 (2006).
14. N. Buddelmeijer, J. Beckwith, A complex of the Escherichia coli cell division proteins FtsL, FtsB and FtsQ forms independently of its localization to the septal region. *Mol. Microbiol.* **52**, 1315–1327 (2004).
15. R. Duman *et al*., Structural and genetic analyses reveal the protein SepF as a new membrane anchor for the Z ring. *Proc. Natl. Acad. Sci. U.S.A.* **110**, E4601–E4610 (2013).
16. M. E. Gündoğdu *et al*., Large ring polymers align FtsZ polymers for normal septum formation. *EMBO J.* **30**, 617–626 (2011).
17. A. Kotiranta, K. Lounatmaa, M. Haapasalo, Epidemiology and pathogenesis of Bacillus cereus infections. *Microbes Infect.* **2**, 189–198 (2000).
18. E. J. Bottone, Bacillus cereus, a volatile human pathogen. *Clin. Microbiol. Rev.* **23**, 382–398 (2010).
19. K. S. Antonation *et al*., Bacillus cereus biovar anthracis causing anthrax in Sub-Saharan Africa—chromosomal monophyly and broad geographic distribution. *PLoS Negl. Trop. Dis.* **10**, e0004923 (2016).
20. A. R. Hoffmaster *et al*., Identification of anthrax toxin genes in a Bacillus cereus associated with an illness resembling inhalation anthrax. *Proc. Natl. Acad. Sci. U.S.A.* **101**, 8449–8454 (2004).
21. C. Hoffmann *et al*., Persistent anthrax as a major driver of wildlife mortality in a tropical rainforest. *Nature* **548**, 82–86 (2017).
22. W. A. Prinz, J. E. Hinshaw, Membrane-bending proteins. *Crit. Rev. Biochem. Mol. Biol.* **44**, 278–291 (2009).
23. N. R. Thanky, D. B. Young, B. D. Robertson, Unusual features of the cell cycle in mycobacteria: polar-restricted growth and the snapping-model of cell division. *Tuberculosis (Edinb.)* **87**, 231–236 (2007).
24. A. A. Velayati, P. Farnia, *Altas of Mycobacterium tuberculosis* (Academic Press, ed. 1, 2016).
25. M. Krupka *et al*., Escherichia coli FtsA forms lipid-bound minirings that antagonize lateral interactions between FtsZ protofilaments. *Nat. Commun.* **8**, 15957 (2017).
26. J. Conti, M. G. Viola, J. L. Camberg, FtsA reshapes membrane architecture and remodels the Z-ring in Escherichia coli. *Mol. Microbiol.* **107**, 558–576 (2018).
27. A. Typas *et al*., Regulation of peptidoglycan synthesis by outer-membrane proteins. *Cell* **143**, 1097–1109 (2010).
28. L. J. Jones, R. Carballido-López, J. Errington, Control of cell shape in bacteria: helical, actin-like filaments in Bacillus subtilis. *Cell* **104**, 913–922 (2001).
29. S. Hussain *et al*., MreB filaments align along greatest principal membrane curvature to orient cell wall synthesis. *eLife* **7**, e32471 (2018).
30. J. Domínguez-Escobar *et al*., Processive movement of MreB-associated cell wall biosynthetic complexes in bacteria. *Science* **333**, 225–228 (2011).
31. E. C. Garner *et al*., Coupled, circumferential motions of the cell wall synthesis machinery and MreB filaments in B. subtilis. *Science* **333**, 222–225 (2011).
32. H. Shi, D. A. Quint, G. M. Grason, A. Gopinathan, K. C. Huang, Chiral twisting in a bacterial cytoskeletal polymer affects filament size and orientation. *Nat. Commun.* **11**, 1408 (2020).

33. P. Riggs, Expression and purification of maltose-binding protein fusions. *Curr. Protoc. Mol. Biol.* **28**, 16.6.1-16.6.14 (1994).
34. M. Yoshimura, T. Oshima, N. Ogasawara, Involvement of the YneS/YgiH and PlsX proteins in phospholipid biosynthesis in both *Bacillus subtilis* and *Escherichia coli*. *BMC Microbiol.* **7**, 69 (2007).
35. D. G. Gibson *et al*., Enzymatic assembly of DNA molecules up to several hundred kilobases. *Nat. Methods* **6**, 343–345 (2009).
36. P. M. Hauser, D. Karamata, A rapid and simple method for Bacillus subtilis transformation on solid media. *Microbiology (Reading)* **140**, 1613–1617 (1994).
37. S. Ishikawa, Y. Kawai, K. Hiramatsu, M. Kuwano, N. Ogasawara, A new FtsZ-interacting protein, YlmF, complements the activity of FtsA during progression of cell division in Bacillus subtilis. *Mol. Microbiol.* **60**, 1364–1380 (2006).
38. A. Valbuena, S. Maity, M. G. Mateu, W. H. Roos, Visualization of single molecules building a viral capsid protein lattice through Stochastic pathways. *ACS Nano* **14**, 8724–8734 (2020).
39. S. Maity *et al*., Caught in the act: Mechanistic insight into supramolecular polymerization-driven self-replication from real-time visualization. *J. Am. Chem. Soc.* **142**, 13709–13717 (2020).
40. J. D. Te Winkel, D. A. Gray, K. H. Seistrup, L. W. Hamoen, H. Strahl, Analysis of antimicrobial-triggered membrane depolarization using voltage sensitive dyes. *Front. Cell Dev. Biol.* **4**, 29 (2016).
41. Y. Gao, M. Wenzel, M. J. Jonker, L. W. Hamoen, Free SepF interferes with recruitment of late cell division proteins. *Sci. Rep.* **7**, 16928 (2017).
42. G. P. van Wezel *et al*., ssgA is essential for sporulation of Streptomyces coelicolor A3(2) and affects hyphal development by stimulating septum formation. *J. Bacteriol.* **182**, 5653–5662 (2000).
43. D. Saeloh *et al*., The novel antibiotic rhodomyrtone traps membrane proteins in vesicles with increased fluidity. *PLoS Pathog.* **14**, e1006876 (2018).
44. M. Wenzel *et al*., New flat embedding method for transmission electron microscopy reveals an unknown mechanism of tetracycline. *bioRxiv*:10.1101/820191 (28 October 2019).